European Journal of Radiology 111 (2019) 6–13

Contents lists available at ScienceDirect

European Journal of Radiology

journal homepage: www.elsevier.com/locate/ejrad

Research article

Differentiating intrapulmonary metastases from different primary tumors via quantitative dual-energy CT based iodine concentration and conventional CT attenuation

Dominik Deniffel*, Andreas Sauter, Julia Dangelmaier, Alexander Fingerle, Ernst J. Rummeny, Daniela Pfeiffer

Department of Diagnostic and Interventional Radiology, Klinikum rechts der Isar, Technical University of Munich, Germany

ARTICLE INFO

Keywords:
Computed tomography
Neoplasm
Pulmonary metastasis
Iodine
Quantitative imaging

ABSTRACT

Introduction: To investigate the utility of quantitative dual-energy spectral CT derived iodine concentration (IC), in comparison with conventional CT attenuation, for the differentiation of pulmonary metastases from different primary malignancies.

Materials and methods: CT scans were performed on a dual-layer spectral CT. We retrospectively evaluated pulmonary metastases of 130 patients (77 men and 53 women, mean age 63, range 22–87) with primary bone (OS) (osteosarcoma; n = 6), breast (invasive-ductal adenocarcinoma; n = 17), colorectal (CRC) (adenocarcinoma; n = 27), head and neck (HNC) (squamous cell carcinoma; n = 17), kidney (RCC) (clear-cell renal cell carcinoma; n = 10), lung (adenocarcinoma; n = 12), pancreato-biliary (PBC) (adenocarcinoma; n = 18), prostate (adenocarcinoma; n = 5), soft tissue (undifferentiated pleomorphic sarcoma; n = 6), skin (malignant melanoma; n = 6), and urinary tract (transitional-cell carcinoma; n = 6) malignancies. Quantitative IC and conventional CT numbers (HU) were extracted and normalized to the thoracic aorta. Differences between the groups were assessed by pairwise t-tests with Holm-Sidak post-hoc p-value adjustment for multiple comparisons. Diagnostic accuracy was evaluated by receiver operating characteristic (ROC) analysis.

Results: Significant differences in IC and HU were noted for pulmonary metastases from RCC (IC: 2.83 mg/ml; HU: 93.12) versus breast cancer (IC: 1.47 mg/ml, adjusted $p < 0.05$; HU: 59.57, adjusted $p < 0.05$), CRC (IC: 1.23 mg/ml, adjusted $p < 0.001$; HU: 49.82, adjusted $p < 0.001$) and HNC (IC: 1.54 mg/ml, adjusted $p < 0.05$; HU: 58.91, adjusted $p < 0.01$). Based on IC alone, significant differences were further observed between metastatic lesions from CRC versus OS (IC: 2.36 mg/ml, adjusted $p < 0.001$), PBC (IC: 2.16 mg/ml, adjusted $p < 0.001$) and urinary tract carcinoma (IC: 2.21 mg/ml, adjusted $p < 0.05$). Based on IC and HU, pulmonary metastases from OS, HNC and RCC may be differentiated from other pulmonary metastases (area under ROC curve, 0.69-0.79). The diagnostic accuracy to discriminate between pulmonary metastases from PBC and those from other malignancies was significantly higher based on IC as compared to HU (area under ROC curve, 0.66; $p < 0.05$); no significant differences in diagnostic accuracy were noted for other differentiations.

Conclusions: Our findings demonstrate the utility of both dual-energy CT derived quantitative IC and conventional CT attenuation values for the differential diagnosis in suspected pulmonary metastases of unknown origin, however giving preference to the use of IC.

1. Introduction

Computed tomography (CT) imaging is the gold standard for detection and evaluation of pulmonary metastases. However, for the further differentiation of nodules suspicious for metastases and to establish the primary tumor, only a few unspecific CT imaging criteria are presently used. These include tumor margins, calcifications, and cavitation [1]. This is not ideal, as the correct identification of the primary

Abbreviations: AUC, area under the receiver operating characteristic curve; CT, computed tomography; DECT, dual-energy computed tomography; HU, Hounsfield units; IC, iodine concentration; ROC, receiver operating characteristic

* Corresponding author at: Department of Diagnostic and Interventional Radiology, Klinikum rechts der Isar, Technical University of Munich, Ismaninger Str. 22, 81675 München, Germany.

E-mail address: dominik.deniffel@tum.de (D. Deniffel).

https://doi.org/10.1016/j.ejrad.2018.12.015
Received 9 October 2018; Received in revised form 30 November 2018; Accepted 13 December 2018
0720-048X/

tumor metastasizing into the lungs may be crucial for the prognosis and future therapy [2].

Recently dual-energy computed tomography (DECT) has shown potential to improve the characterization of pulmonary lesions. DECT techniques can be based on various scanner concepts, and include dual-source CT scanners, rapid kVp-switching of a single X-ray tube or dual-layer spectral CT detectors [3]. Amongst several possible applications based on DECT data, the most widely used are iodine distribution maps, yielding quantitative iodine concentrations (IC) or iodine densities in the tissue of interest, utilized as a surrogate of vascularization [4]. Recent phantom studies confirmed high accuracy of IC obtained by the different DECT platforms [5,6]. However, dual-layer CT and rapid-kVp-switching CT systems provided slightly more accurate results [6].

DECT-derived IC or iodine densities have been successfully applied for the differentiation of primary lung cancer [7,8], to evaluate therapy response in lung cancer [9] and to discriminate benign from malignant pulmonary nodules, including pulmonary metastases [10–13]. Most of these previous studies did not further quantitatively sub-classify metastatic lesions in terms of the location and histology of their primary tumors.

The purpose of our study was to investigate the diagnostic utility of the DECT-derived quantitative imaging biomarker IC and conventional CT attenuation values for the differentiation of pulmonary metastases from different primary neoplasms. We hypothesized that quantitative DECT imaging biomarkers obtained from a single venous phase scan protocol could improve the differentiation of metastatic pulmonary lesions compared to conventional CT attenuation measurements.

2. Materials and methods

2.1. Patients

This retrospective, single-center study was approved by our institutional review board, and a waiver of informed consent was obtained. We analyzed spectral CT imaging studies performed at our department for staging of a suspected or known malignancy between September 2016 and April 2018. By performing a computerized search within the radiology information system, we identified 536 patients with suspected pulmonary metastases. 191 patients with histopathologically confirmed primary tumors demonstrated new pulmonary metastases within the observation period. When histopathological analysis of the metastatic lesion following biopsy and/or surgical resection was not available (87 patients), the final diagnosis was proven by clinical follow-up > 6 months demonstrating progression of the pulmonary metastases, defined by the appearance of new lesions or > 20% progression in size. 52 patients who had already received specific treatment for pulmonary metastases (systemic, local) prior to the CT scan were excluded from further analysis. 9 additional patients were excluded due to insufficient lesion size (diameter < 5 mm) to avoid partial volume averaging. We finally included 130 patients in our analysis with the following primary neoplasms: osteosarcoma (n = 6), invasive-ductal adenocarcinoma of the breast (n = 17), colorectal adenocarcinoma (n = 27), squamous-cell carcinoma of the head and neck (n = 17), clear-cell renal cell carcinoma (n = 10), adenocarcinoma of the lung (n = 12), pancreato-biliary adenocarcinoma (n = 18), adenocarcinoma of the prostate (n = 5), undifferentiated pleomorphic sarcoma (n = 6), malignant melanoma (n = 6), transitional-cell carcinoma (n = 6). This group comprised 77 men and 53 women with a mean age of 63 (range 22 to 87). The mean size of pulmonary metastases was 1498 mm^3 (range 96 to 16,876). Fig. 1 shows the patient accrual process from target cohort to final study population with inclusion and exclusion criteria.

2.2. CT examination protocol

All patients were examined using a dual-layer spectral CT (IQon; Philips Healthcare, The Netherlands) using the same routine protocol. Contrast material (Iomeprol, Imeron 400 MCT, 400 mg/ml; Bracco Imaging Deutschland GmbH, Konstanz, Germany) was administered intravenously using a standard dosage of 1.2 ml per KG body weight at a flow rate of 2–2.5 ml/s, followed by 30 mL of saline solution at the same flow rate. Scan delay time was 70 s after the start of contrast medium injection, considered a venous phase scan. The following scanning parameters were used: 120 kVp; automatic tube current selection with resulting exposures of 37–84 mA s; 512 × 512 matrix; scan FOV 400 mm; collimation 64 × 0.625 mm; reconstructed slice thickness and interval 0.9 mm/0.9 mm with a soft tissue kernel). Conventional and spectral basis images were reconstructed using the iDose4 (Philips Healthcare, The Netherlands) reconstruction algorithm at level 6 (maximum level 7). The mean volume-weighted CT dose index ($CTDI_{vol}$), and dose-length product (DLP) for the complete protocol were 4.4 mGy and 180 mGy*cm, respectively, corresponding to an effective dose of 2.5 mSv (conversion factor 0.014).

2.3. Quantitative analysis

Quantitative analysis of spectral CT images using commercially available software (IntelliSpace Portal v. 10.1, Philips Healthcare, USA) was performed in consensus by a resident fellow in radiology (3 years of radiology experience) and a senior radiologist (11 years of radiology experience), who were blinded for the histological diagnosis of the primary tumor. In every patient, lesion volume was semi-automatically segmented in the axial plane on virtual non-contrast images, derived from spectral CT, with soft tissue window settings, creating a volume-of-interest of the pulmonary metastasis. According to previous studies and our own experiences, segmentation of lung lesions in virtual non-contrast images as compared to contrast-enhanced images results in a significant volume reduction [14]. By this approach, we aimed to minimize 'volume averaging' effects by excluding the lesion's peripheral voxels at the cost of an underestimation of the true lesion volume. Based on recommendations from a recent phantom study, partial volume effects given our reconstructed slice thickness of 0.9 mm would allow for acceptable detection and characterization of a minimum spherical lesion diameter of 1.5 mm, corresponding to a volume of 1.77 mm^3 [15]. The smallest lesion included in our series measured 96 mm^3, since the software algorithm failed to detect the contours reliably in smaller lesions. A circular two-dimensional region-of-interest was manually placed in the descending aorta. Exploiting the dual-layer concept, the software simultaneously provides conventional polychromatic CT images and iodine-density maps. Mean values of the following parameters were obtained and recorded for each patient: IC in mg/ml and attenuation values in HU on conventional CT images. To account for hemodynamic inter-patient variations, the measured parameter values in the volume-of-interest of the pulmonary metastasis were normalized using the following formula: (parameter value 'pulmonary metastasis') x [(mean parameter value 'thoracic aorta' of all patients) / (individual parameter value 'thoracic aorta')]. By this approach, instead of using ratios as previously described [11,16], we obtained normalized values in the actual unit of measurement.

2.4. Statistical analysis

Statistical differences between means of measured IC and HU in histology groups were analyzed by pairwise t-tests followed by Holm-Sidak post-hoc correction for multiple comparisons. We further compared the diagnostic accuracy of IC and HU to discriminate between pulmonary metastases from a specific primary tumor and those of other malignancies. Accuracy was measured by the area under the corresponding receiver operating characteristic curve (AUC). Differences between the AUCs were compared using the method of DeLong et al. [17]. Statistical significance was considered at a P value of < 0.05. Statistical analyses were performed using the software applications

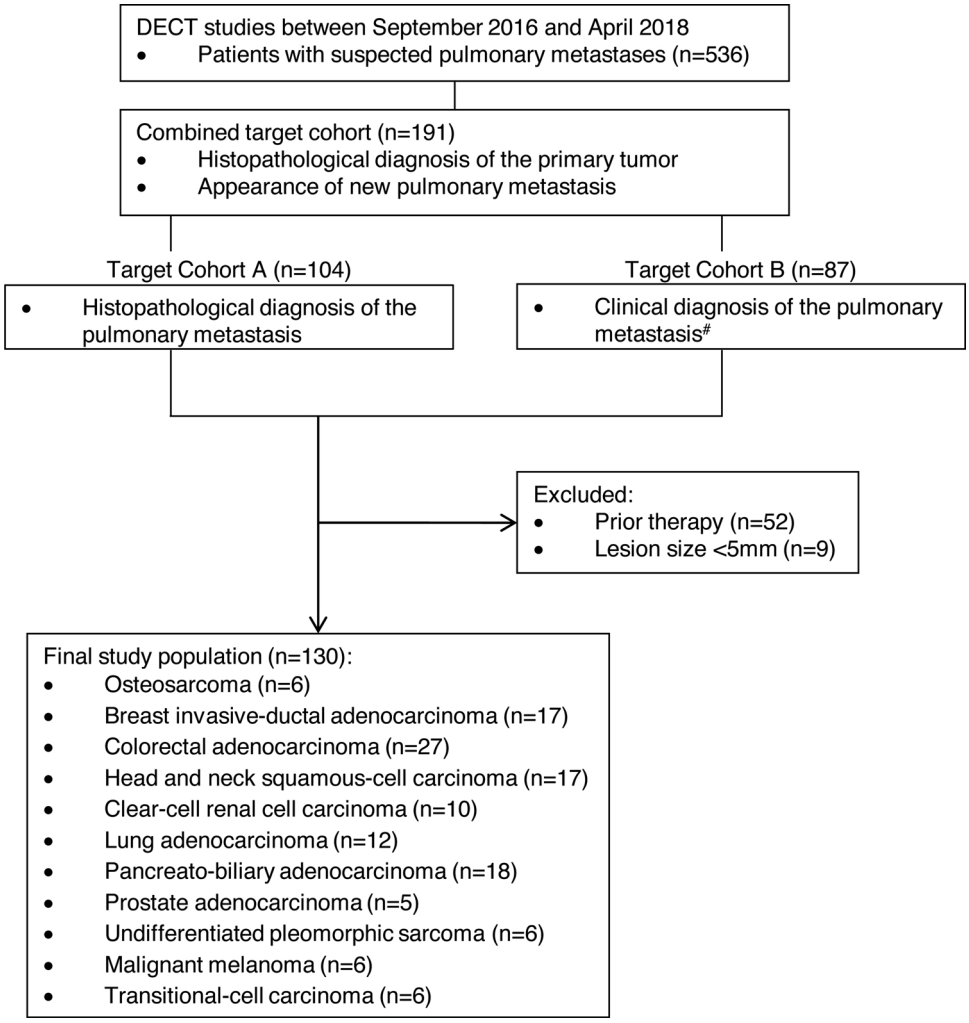

Fig. 1. Flowchart shows patient recruitment process from target cohort to final study population with inclusion and exclusion criteria.

GraphPad Prism (Version 7, GraphPad Software Inc., La Jolla, CA), MedCalc (Version 7.4.4.1, MedCalc Software, Mariakerke, Belgium) and IBM SPSS Statistics (Version 24, IBM Corp., Armonk, N.Y., USA).

3. Results

Representative results for two patients with pulmonary metastases from rectal adenocarcinoma and cholangiocellular carcinoma are presented in Fig. 2 a–d.

3.1. Quantitative iodine concentration and conventional CT attenuation for pulmonary metastases from different primaries

Quantitative results for the dual-energy CT derived IC and conventional CT attenuation values in HU for pulmonary metastases from different primary tumor locations and entities are provided in Table 1 and illustrated in Fig. 3, a–b.

3.2. Pairwise comparisons of mean iodine concentration and conventional CT attenuation values

Supplemental file 1, table S1 demonstrates the results of pairwise comparisons of mean IC and HU values, reported in mean differences with standard error, non-adjusted p-values from pairwise t-tests and adjusted p-values after Holm-Sidak post-hoc correction for multiple comparisons. Significant differences in IC and HU were observed for metastatic pulmonary lesions from renal cell carcinoma versus carcinoma of the breast (IC/HU: adjusted $p < 0.05$), colorectum (IC/HU: adjusted $p < 0.001$) and head and neck (IC: adjusted $p < 0.05$; HU: adjusted $p < 0.01$). Metastatic lesions from colorectal adenocarcinoma further differed significantly in the quantitative IC imaging biomarker compared to those from osteosarcoma (adjusted $p < 0.001$), pancreato-biliary (adjusted $p < 0.001$) and urinary tract carcinoma (adjusted $p < 0.05$). Results from pairwise comparisons are illustrated in Fig. 3, a–b.

3.3. Comparison of diagnostic accuracies by receiver operating characteristic curve analysis

We assessed the diagnostic accuracy of mean IC and HU values to discriminate pulmonary metastases from a particular primary tumor from those of various other malignancies. Receiver operating characteristic (ROC) curves are presented in Fig. 4, a–b, corresponding AUCs from ROC curve analysis are provided in Table 2. AUC values for the differentiation of osteosarcoma (AUC IC: 0.74; AUC HU: 0.7), head and neck squamous cell carcinoma (AUC IC: 0.75; AUC HU: 0.69), clear-cell renal cell carcinoma (AUC IC: 0.75; AUC HU: 0.69) and pancreato-biliary adenocarcinoma (AUC IC: 0.66) are significantly different from 0.5 ($p < 0.05$, respectively), which indicates that they are useful diagnostic tests in the given situations. For pulmonary metastases originating from other tumors, discrimination is not reliably feasible based on IC and HU measurements. For the differentiation of

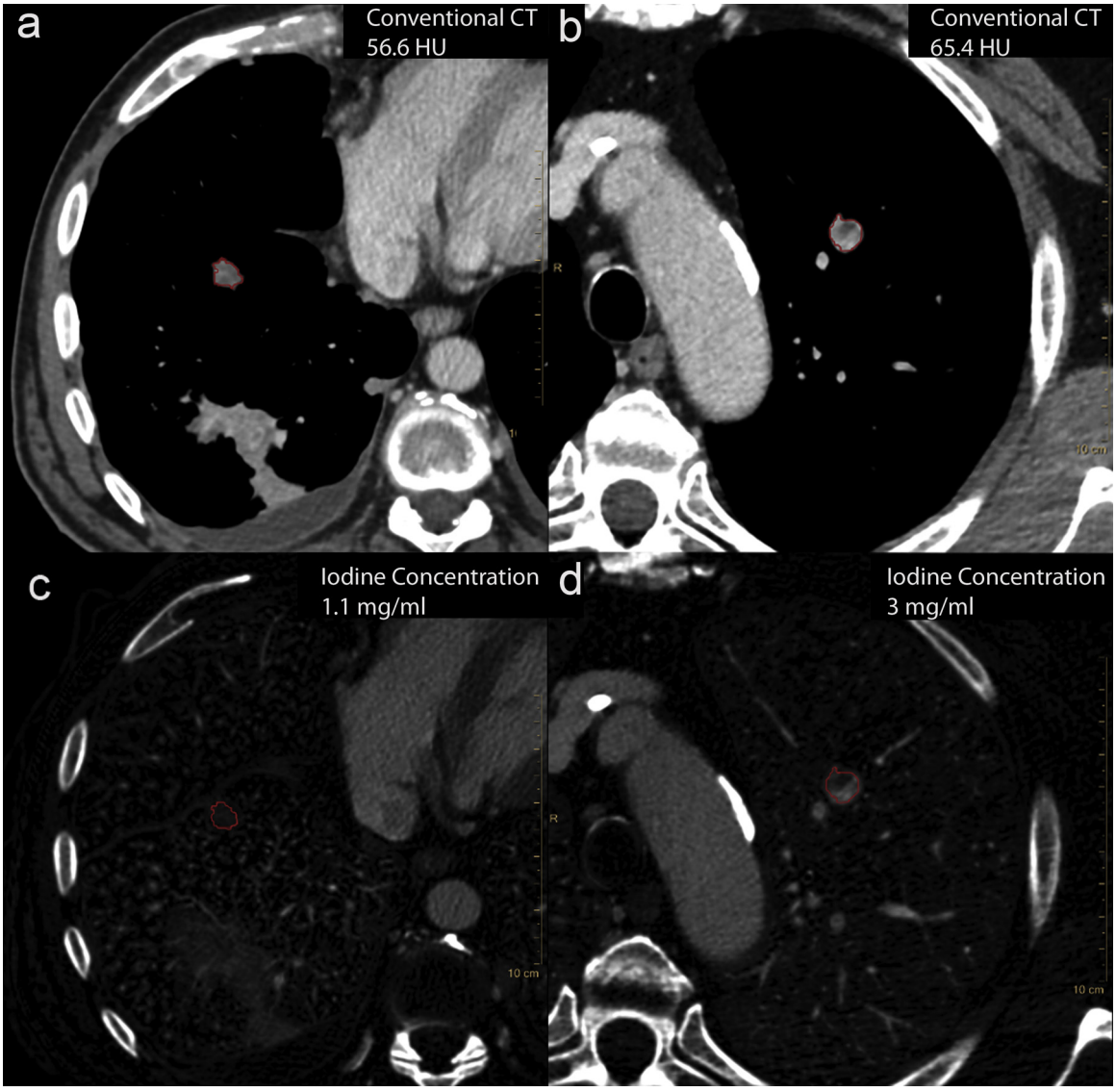

Fig. 2. Dual-energy spectral CT studies of pulmonary metastases in a 52-year-old woman with rectal adenocarcinoma (**a, c**) and a 70-year-old man with cholangiocarcinoma (**b, d**). Conventional CT images (**a, b**) and quantitative iodine concentration maps (**c, d**) with obtained quantitative parameter values are given for the delineated volume-of-interest (red color). The differences between the metastases become more pronounced when the quantitative iodine concentration biomarker is considered.

pulmonary pancreato-biliary adenocarcinoma metastases from other pulmonary metastases, the diagnostic accuracy based on HU values was significantly lower as compared to IC ($p < 0.05$); no significant differences in diagnostic accuracy were noted for other differentiations. Results of ROC curve analysis for the distinction of urinary tract carcinoma metastases from other pulmonary metastases are not

Table 1
Mean values of iodine concentration and conventional HU of lung metastases from different primary tumors.

Primary Location	Histology	Sample n =	IC (mg/ml)	HU
bone	osteosarcoma	6	2.36 ± 0.66 [1.66-3.05]	78.71 ± 18.82 [58.96-98.46]
breast	invasive-ductal adenocarcinoma	17	1.47 ± 0.58 [1.17-1.77]	59.57 ± 18.7 [49.96-69.19]
colorectum	adenocarcinoma	27	1.23 ± 0.547 [1.01-1.44]	49.82 ± 22.04 [41.1-58.54]
head and neck	squamous cell carcinoma	17	1.54 ± 0.45 [1.31-1.77]	58.91 ± 15.68 [50.85-66.97]
kidney	clear-cell carcinoma	10	2.83 ± 1.22 [1.96-3.7]	93.12 ± 22.46 [77.05-109.2]
lung	adenocarcinoma	12	1.6 ± 0.9 [1.03-2.17]	53.76 ± 28.9 [35.4-72.12]
pancreato-biliary tract	adenocarcinoma	18	2.16 ± 0.742 [1.79-2.53]	66.81 ± 25.28 [54.25-79.38]
prostate	adenocarcinoma	5	1.63 ± 0.44 [1.08-2.17]	62.26 ± 16.7 [41.53-82.99]
soft tissue	undifferentiated pleomorphic sarcoma	6	2.14 ± 0.92 [1.18-3.1]	81.12 ± 29.85 [49.79-112.4]
skin	melanoma	6	2.28 ± 1.19 [1.04-3.53]	73.95 ± 26.31 [46.34-101.6]
urinary tract	transitional cell carcinoma	6	2.21 ± 0.61 [1.57-2.85]	73.66 ± 19.87 [52.8-94.51]

Listed are mean values ± standard deviation and 95% confidence intervals of the mean in brackets. Primary tumors are specified by their primary location and histology. IC indicates iodine concentration on dual-energy CT; HU the conventional CT attenuation values in Hounsfield units.

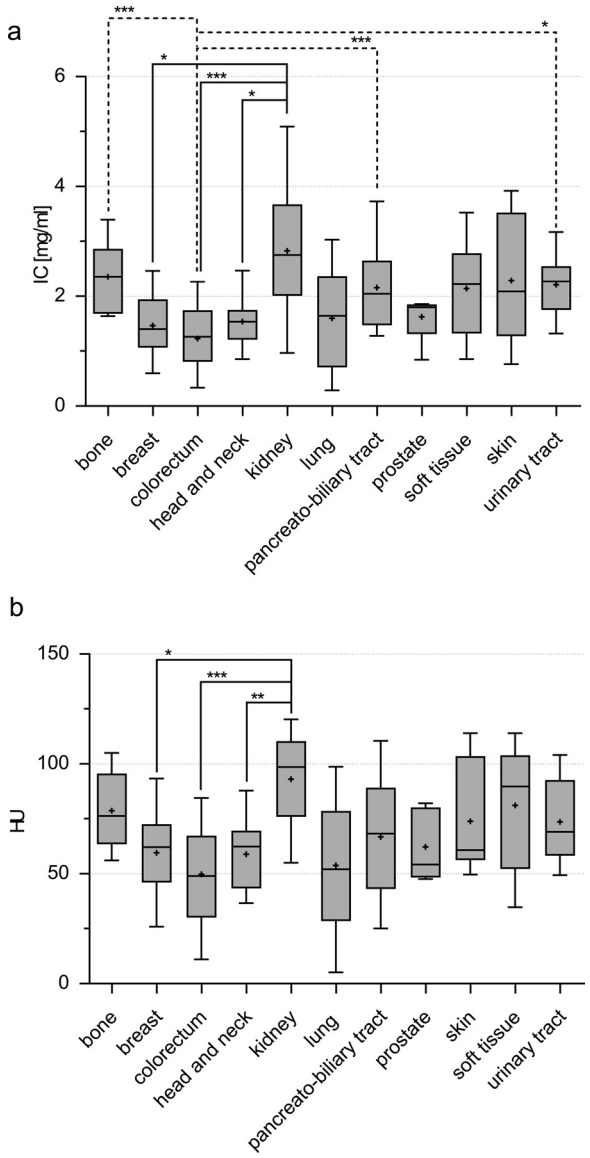

Fig. 3. Quantitative results for the dual-energy CT derived iodine concentration and conventional CT attenuation values. (**a**) Median and mean values of iodine concentration (IC), (**b**) conventional Hounsfield unit values (HU), both with quartiles, minimum and maximum values, for pulmonary metastases from primary bone (osteosarcoma), breast (invasive-ductal adenocarcinoma), colorectal (adenocarcinoma), head and neck (squamous cell carcinoma), kidney (clear-cell renal cell carcinoma), lung (adenocarcinoma), pancreato-biliary (adenocarcinoma), prostate (adenocarcinoma), soft tissue (undifferentiated pleomorphic sarcoma), skin (malignant melanoma) and urinary tract (transitional-cell carcinoma) malignancies. The plus indicates the mean value. Presented are results of pairwise t-tests followed by Holm-Sidak post-hoc correction for multiple comparisons. For both quantitative imaging biomarkers, metastases from kidney carcinoma differ significantly compared to those of various other primary tumors. For IC alone, additional significant differences between colorectal carcinoma versus osteosarcoma, pancreato-biliary and urinary tract carcinoma are observed. * indicates an adjusted P value of < 0.05, ** < 0.01, *** < 0.001.

conclusive. The AUC based on IC is significantly different from 0.5 ($p < 0.05$), which is not the case for HU; conversely, no significant differences between the AUCs based on the two different parameters were noted ($p = 0.51$).

4. Discussion

First, this study provides a reference range of the quantitative IC values derived from DECT imaging and conventional HU values for a variety of pulmonary metastases. We could demonstrate significant differences for metastases of renal cell carcinoma versus those of breast, colorectal and head and neck carcinoma and metastases of colorectal carcinoma versus osteosarcoma, pancreato-biliary and urinary tract carcinoma. Based on both IC and HU, pulmonary metastases from osteosarcoma, head and neck and kidney carcinoma may be differentiated from other pulmonary metastases. Based on HU, differences between the groups were less pronounced with fewer significantly different pairings and a significantly lower diagnostic accuracy to discriminate between pulmonary metastases from pancreato-biliary and those from other malignancies. Our findings support the use of quantitative DECT imaging biomarkers for the diagnostic work-up of suspected pulmonary metastatic lesions. However, in the majority of cases, a definite differentiation between all histologic subtypes is not feasible. An advantage of DECT derived IC over conventional HU values was consistently demonstrated by several previous studies, suggesting a more reliable detection of subtle enhancement differences [11,12,18–20]. Phantom studies comparing modern dual-energy and spectral CT systems from different vendors confirmed excellent accuracy and agreement of IC measurements [5,6]. CT attenuation profiles, however, differed significantly in a recent study [5], which substantiates the use of IC for clinical routine. Iodine uptake can be utilized as a surrogate marker for tumor perfusion and angiogenesis [4]. The degree of pulmonary vascular neogenesis varies considerably between metastases from different tumors, which tend to duplicate the vasculature architecture of their primary tumor [21,22], which may finally result in similar enhancement patterns. Accordingly, tumors typically considered to result in hypervascular (e.g. clear-cell renal cell carcinoma) or hypovascular (e.g. colorectal, breast or prostate adenocarcinoma) metastases in the liver [23,24] show similar enhancement patterns in pulmonary metastatic lesions in our series. Conversely, hypervascular liver metastases have also been reported in patients with colon, gastric and breast adenocarcinoma [25], although less frequently, which provides a possible explanation for the relatively large within-group variances in our series. Several previous works have demonstrated that reliable discrimination of benign from malignant pulmonary nodules can be achieved by conventional [26,27] or DECT [10,11] imaging. But there has not yet been a larger effort to use this approach to sub-classify the involved malignant lesions. So far, there is only one recent DECT research study that has evaluated the iodine uptake of pulmonary metastases from different primary tumors [28]. The statistical assessment of this study was focused on the assessment of kinetic contrast enhancement profiles in a dual-phase acquisition protocol. The scope of this report was limited in terms of a relatively small sample size (70 patients) and few tumor entities (six). Consistent with our report, metastases from colorectal adenocarcinomas yielded low, lung carcinomas intermediate and sarcomas conspicuous contrast enhancement. By contrast, malignant melanomas, traditionally considered to cause hypervascular metastases [29], showed low enhancement on venous phase in this previous versus relatively high IC in our study. The results of iodine uptake in this previous report were not presented in the standard unit milligram per volume, thereby preventing quantitative comparison with our results, and precluding their use as reference values for institutions working with different vendor platforms. In general, finding the primary site of a suspected metastatic lesion is imperative to permit the planning of treatment approaches [2]. The usual diagnostic approach to suspicious lung lesions detected on chest x-ray or CT includes surgical resection or tissue sampling via biopsy, e.g. transbronchial or CT-guided. Surgical resection carries considerable risks for patients with multiple comorbidities and nodules located in proximity to the mediastinum, major vessels or behind the heart can be technically challenging and dangerous to biopsy. Moreover, biopsy

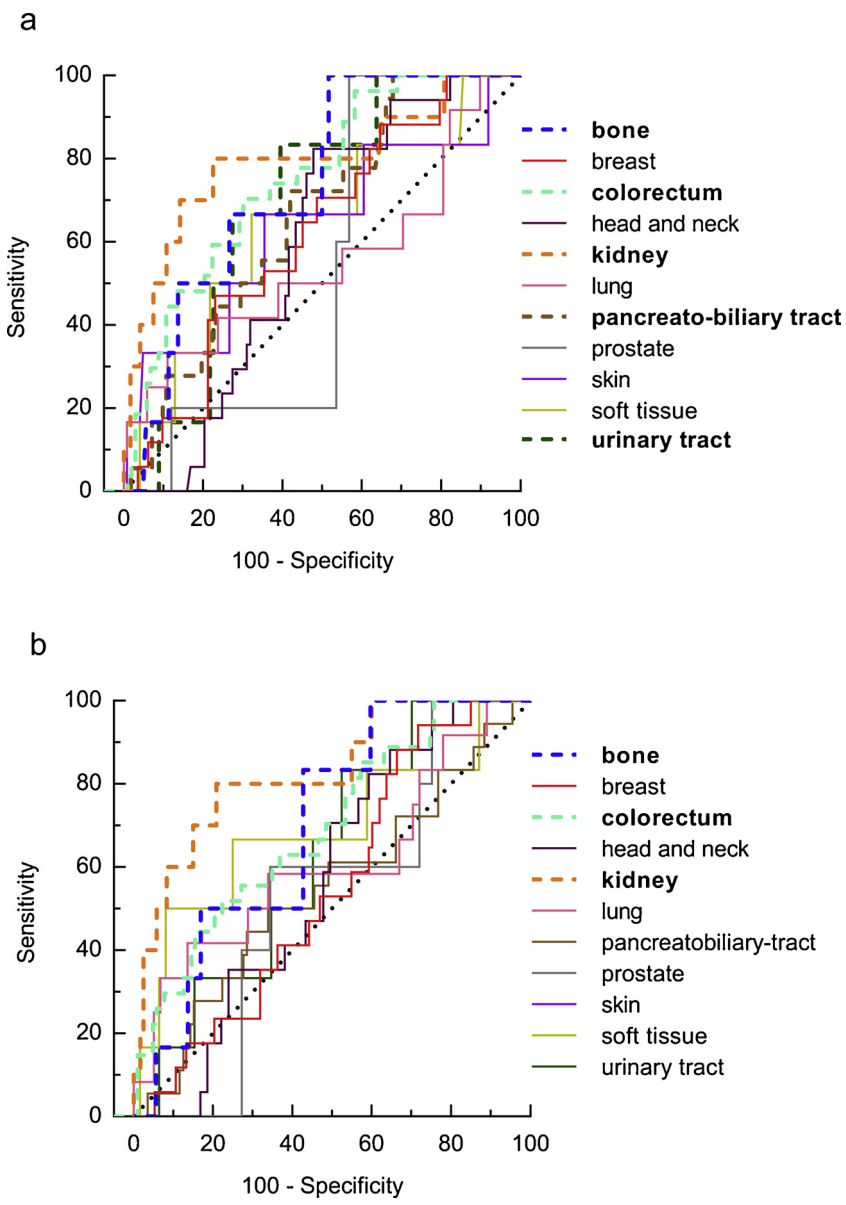

Fig. 4. Receiver operating characteristic (ROC) curves based on (**a**) iodine concentration (IC) and (**b**) conventional CT attenuation values in Hounsfield units (HU). The ROC curves were constructed for discrimination of pulmonary metastases from a specific primary tumor versus metastases from other malignancies. Bold dashed lines represent ROC curves of diagnostic tests that can distinguish between the two groups (area under the ROC curve significantly different from 0.5, $p < 0.05$).

results may be equivocal requiring rebiopsy. Clinical situations where integration of IC derived from DECT imaging could add additional value to the diagnostic work-up include metastatic cancer of unknown primary and suspected pulmonary metastases in single or multiple known extrapulmonary malignancies. Pulmonary metastases with occult primary present a frequent diagnostic and therapeutic challenge. The lack of a detectable primary tumor in conventional imaging traditionally involves a series of investigations to locate the primary site of the tumor. These diagnostic studies include mammograms, panendoscopy of the upper aerodigestive pathways, bronchoscopy, gastroscopy, colonoscopy, diagnostic laparotomy, or 18F-FDG-PET. Many of these tests are not only painful or distressing to patients, but also unsuccessful in locating the primary location of metastatic disease. Therefore extensive unguided clinical evaluation may put a substantial financial burden on the health care system with a negative cost-to-benefit ratio [30,31]. The ranges of IC for different metastatic pulmonary lesions provided in our study help to favor a specific primary tumor site and thus avoid unnecessary diagnostic procedures, particularly in patients where tissue sampling from the suspected lung metastasis is unsafe, infeasible, or otherwise unsuccessful. Based on the reference parameter values in our study, metastatic lesions with relatively low IC values suggesting colorectal carcinoma may thus directly lead to a colonoscopy whereas relatively high IC values may guide further diagnostics to systematic skin examination and additional abdominal imaging for suspected malignant melanoma and renal cell carcinoma, respectively. Another clinical situation that benefits from DECT imaging is the appearance of pulmonary nodules in patients with a known extrapulmonary malignancy. Many patients suspected to have pulmonary metastases are assigned to palliative treatment, which dramatically changes the clinical management and prognosis. So far, there has been no consensus or guideline whether tissue sampling with the potential risks involved should be performed in these cases. IC values characteristic of the known primary may avoid sampling, whereas non-characteristic IC values may support clinicians in their decision to obtain tissue samples for accurate diagnosis. Pulmonary lesions in these patients may harbor a primary lung tumor or metastasis of a yet

Table 2
Results of ROC Curve Analysis based on iodine concentration and conventional HU.

Primary Location	Histology	AUC IC	AUC HU	Comparison p-value
bone	osteosarcoma	**0.74** [0.65-0.81]	**0.7** [0.61-0.78]	P = 0.378
breast	invasive-ductal adenocarcinoma	0.62 [0.53-0.70]	0.55 [0.46-0.64]	P = 0.172
colorectum	adenocarcinoma	0.59 [0.50-0.68]	0.57 [0.48-0.65]	P = 0.618
head and neck	squamous cell carcinoma	**0.75** [0.67-0.82]	**0.69** [0.61-0.77]	P = 0.144
kidney	clear-cell carcinoma	**0.79** [0.71-0.86]	**0.83** [0.75-0.89]	P = 0.254
lung	adenocarcinoma	0.55 [0.46-0.64]	0.61 [0.52-0.69]	P = 0.068
pancreato-biliary tract	adenocarcinoma	**0.66** [0.57-0.74]	0.55 [0.46-0.63]	**P = 0.012**
prostate	adenocarcinoma	0.53 [0.45-0.62]	0.53 [0.44-0.62]	P = 0.958
soft tissue	undifferentiated pleomorphic sarcoma	0.64 [0.55-0.72]	0.69 [0.60-0.77]	P = 0.0967
skin	melanoma	0.63 [0.55-0.72]	0.59 [0.50-0.68]	P = 0.600
urinary tract	transitional cell carcinoma	**0.69** [0.61-0.77]	0.63 [0.54-0.71]	P = 0.507

ROC indicates receiver operating characteristic; AUC, area under the receiver operating characteristic curve; IC, iodine concentration on dual-energy computed tomography; HU, conventional computed tomography attenuation values in Hounsfield units. ROC curves were constructed for Discrimination of pulmonary metastases from a specific primary tumor versus metastases from other malignancies using IC from dual-energy CT and HU from conventional CT. Listed are AUC values with binomial exact 95% confidence intervals in brackets and p-values from the comparison of AUCs based on IC and HU. Primary tumors are specified by their primary location and histology. AUC values significantly different from 0.5 ($P < 0.05$), suggesting useful diagnostic tests, are highlighted in boldface. P-values set in boldface indicate statistical significant differences (< 0.05).

unknown additional malignancy. Synchronous and metachronous malignancies are relatively common in several types of primary cancers, due to genetic susceptibility and exposure to carcinogens including chemo- and/or radiotherapy [32] and should thus always be considered in follow-up imaging studies. Another diagnostic challenge involves patients with multiple primary tumors presenting with suspicious pulmonary lesions. In this patient group, our provided IC ranges may be advantageous to determine which of the known primary tumors metastasizes to the lungs and should, therefore, be targeted in treatment planning. Several limitations of our present study need to be acknowledged. First, pathological confirmation was not available for all of the analyzed pulmonary metastases. However, the strict inclusion criteria for patients and lesions without histopathological diagnosis reduce this risk of erroneous diagnoses to a minimum. Second, not all common primary tumors, frequently metastasizing to the lungs, are present in our cohort, e.g. malignancies of the uterus or thyroid gland [33]. Furthermore, no benign pulmonary lesions and no primary lung tumors are included in our study. Particularly the discrimination of inflammatory from neoplastic masses and solitary lung metastasis from primary lung cancer can create diagnostic difficulties, which are not addressed in our investigation. Third, we used a single-phase protocol, while many investigators have applied dual- or multiphase imaging protocols for the evaluation of pulmonary lesions, both on conventional [26,34] and DECT [10,11,35]. The additional values of multiphase protocols are the increased chance that the image acquisition coincides with the tumor's characteristic peak iodine uptake and the simultaneous assessment of contrast kinetics, previously suggested to improve differential diagnosis of pulmonary lesions [13,36]. Fourth, considering the exploratory character of this research, and with regards to the wide ranges of standard deviations within the groups, conclusions especially drawn from smaller and heterogeneous subgroups are tentative and need confirmation. Further sub-classification and increased patient numbers taking into account the histological grade or even genomic subtypes would presumably homogenize the results and improve the differentiation. Support for this hypothesis comes from previous studies demonstrating significant differences in IC between tumors of different histological grade [37,38]. Fifth, this study only includes one single imaging parameter derived from DECT. The aim of this exploratory study was to demonstrate the overall feasibility to differentiate pulmonary metastases based on IC, introduced as a promising quantitative imaging biomarker. Recently, radiomics approaches using high-throughput extraction of a large amount of quantitative imaging features have shown potential for histological sub-typing of primary lung tumors [39] and discriminating malignant from benign pulmonary nodules [40,41]. Integrating IC and additional DECT derived parameters in radiomics feature sets opens up a host of possible future studies.

5. Conclusions

In conclusion, the findings of our study confirm the utility of both the DECT-derived quantitative parameter IC and conventional HU for the distinction between pulmonary metastases of various malignancies, however giving preference to the use of IC. Our data give an overview of the expected ranges of quantitative parameter values which may help to narrow down the differential diagnosis and guide further diagnostic approaches, crucial for the prognosis and future therapy.

Authors' contributions

DP supervised and conceived the project. DD and DP post-processed and analyzed the CT studies. DD wrote the manuscript with support from DP. DD performed the statistical analysis. AS, JD, AF and EJR provided editorial advice. All authors have read and approved the final manuscript.

Competing interests

The authors certify that they have no conflicts of interest.

Funding information

No funding was involved in this study.

Ethics approval and consent to participate

This retrospective, single-center study was approved by our institutional review board, and a waiver of informed consent was obtained.

Acknowledgements

We would like to thank Dr. Bernhard Haller from the Institute of Medical Statistics and Epidemiology of the Technical University of Munich, who provided statistical advice and Neonila Deniffel and Andreas Zorn who assisted with graphics.

Appendix A. Supplementary data

Supplementary material related to this article can be found, in the

online version, at doi:https://doi.org/10.1016/j.ejrad.2018.12.015.

References

[1] S.D. Davis, CT evaluation for pulmonary metastases in patients with extrathoracic malignancy, Radiology. 180 (1991) 1–12, https://doi.org/10.1148/radiology.180.1.2052672.

[2] K.Y. Yoneda, S. Louie, D.K. Shelton, Approach to pulmonary metastases, Curr. Opin. Pulm. Med. 6 (2000) 356–363 (Accessed 8 May 2018), http://www.ncbi.nlm.nih.gov/pubmed/10912646.

[3] C.H. McCollough, S. Leng, L. Yu, J.G. Fletcher, Dual- and multi-energy CT: principles, technical approaches, and clinical applications, Radiology. 276 (2015) 637–653, https://doi.org/10.1148/radiol.2015142631.

[4] X. Chen, Y. Xu, J. Duan, C. Li, H. Sun, W. Wang, Correlation of iodine uptake and perfusion parameters between dual-energy CT imaging and first-pass dual-input perfusion CT in lung cancer, Medicine (Baltimore). 96 (2017) e7479, https://doi.org/10.1097/MD.0000000000007479.

[5] H. Kim, J.M. Goo, C.K. Kang, K.J. Chae, C.M. Park, Comparison of iodine density measurement among dual-energy computed tomography scanners from 3 vendors, Invest. Radiol. 53 (2018), https://doi.org/10.1097/RLI.0000000000000446.

[6] T. Sellerer, P.B. Noël, M. Patino, A. Parakh, S. Ehn, S. Zeiter, J.A. Holz, J. Hammel, A.A. Fingerle, F. Pfeiffer, D. Maintz, E.J. Rummeny, D. Muenzel, D.V. Sahani, Dual-energy CT: a phantom comparison of different platforms for abdominal imaging, Eur. Radiol. 28 (2018) 2745–2755, https://doi.org/10.1007/s00330-017-5238-5.

[7] J.Y. Son, H.Y. Lee, J.-H. Kim, J. Han, J.Y. Jeong, K.S. Lee, O.J. Kwon, Y.M. Shim, Quantitative CT analysis of pulmonary ground-glass opacity nodules for distinguishing invasive adenocarcinoma from non-invasive or minimally invasive adenocarcinoma: the added value of using iodine mapping, Eur. Radiol. 26 (2016) 43–54, https://doi.org/10.1007/s00330-015-3816-y.

[8] G. Wang, C. Zhang, M. Li, K. Deng, W. Li, Preliminary application of High-definition computed tomographic gemstone spectral imaging in lung cancer, J. Comput. Assist. Tomogr. 38 (2014) 77–81, https://doi.org/10.1097/RCT.0b013e3182a21633.

[9] J. Baxa, A. Vondráková, T. Matoušková, O. Růžičková, B. Schmidt, T. Flohr, M. Sedlmair, J. Ferda, Dual-phase dual-energy CT in patients with lung cancer: assessment of the additional value of iodine quantification in lymph node therapy response, Eur. Radiol. 24 (2014) 1981–1988, https://doi.org/10.1007/s00330-014-3223-9.

[10] E.J. Chae, J.-W. Song, B. Krauss, K.-S. Song, C.W. Lee, H.J. Lee, J.B. Seo, Dual-energy computed tomography characterization of solitary pulmonary nodules, J. Thorac. Imaging. 25 (2010) 301–310, https://doi.org/10.1097/RTI.0b013e3181e16232.

[11] Y. Zhang, J. Cheng, X. Hua, M. Yu, C. Xu, F. Zhang, J. Xu, H. Wu, Can spectral CT imaging improve the differentiation between malignant and benign solitary pulmonary nodules? PLoS One. 11 (2016) e0147537, , https://doi.org/10.1371/journal.pone.0147537.

[12] E.J. Chae, J.-W. Song, J.B. Seo, B. Krauss, Y.M. Jang, K.-S. Song, Clinical utility of dual-energy CT in the evaluation of solitary pulmonary nodules: initial experience, Radiology. 249 (2008) 671–681, https://doi.org/10.1148/radiol.2492071956.

[13] J. Altenbernd, A. Wetter, L. Umutlu, S. Hahn, A. Ringelstein, M. Forsting, T. Lauenstein, Dual-energy computed tomography for evaluation of pulmonar y nodules with emphasis on metastatic lesions, Acta Radiol. 57 (2016) 437–443, https://doi.org/10.1177/0284185115582060.

[14] A.M. den Harder, F. Bangert, R.W. van Hamersvelt, T. Leiner, J. Milles, A.M.R.R. Schilham, M.J. Willemink, P.A. de Jong, The effects of iodine attenuation on pulmonary nodule volumetry using novel dual-layer computed tomography reconstructions, Eur. Radiol. 27 (2017) 5244–5251, https://doi.org/10.1007/s00330-017-4938-1.

[15] P. Monnin, N. Sfameni, A. Gianoli, S. Ding, Optimal slice thickness for object detection with longitudinal partial volume effects in computed tomography, J. Appl. Clin. Med. Phys. 18 (2017) 251–259, https://doi.org/10.1002/acm2.12005.

[16] V. González-Pérez, E. Arana, M. Barrios, A. Bartrés, J. Cruz, R. Montero, M. González, C. Deltoro, E. Martínez-Pérez, K. De Aguiar-Quevedo, M. Arrarás, Differentiation of benign and malignant lung lesions: dual-energy computed tomography findings, Eur. J. Radiol. 85 (2016) 1765–1772, https://doi.org/10.1016/j.ejrad.2016.07.019.

[17] E.R. DeLong, D.M. DeLong, D.L. Clarke-Pearson, Comparing the areas under two or more correlated receiver operating characteristic curves: a nonparametric approach, Biometrics 44 (1988) 837–845 (Accessed 2 September 2017), http://www.ncbi.nlm.nih.gov/pubmed/3203132.

[18] K. Hellbach, A. Sterzik, W. Sommer, M. Karpitschka, N. Hummel, J. Casuscelli, M. Ingrisch, M. Schlemmer, A. Graser, M. Staehler, Dual energy CT allows for improved characterization of response to antiangiogenic treatment in patients with metastatic renal cell cancer, Eur. Radiol. 27 (2017) 2532–2537, https://doi.org/10.1007/s00330-016-4597-7.

[19] D. Marin, D. Davis, K. Roy Choudhury, B. Patel, R.T. Gupta, A. Mileto, R.C. Nelson, Characterization of small focal renal lesions: diagnostic accuracy with single-phase contrast-enhanced dual-energy CT with material attenuation analysis compared with conventional attenuation measurements, Radiology 284 (2017) 737–747, https://doi.org/10.1148/radiol.2017161872.

[20] D. Muenzel, G.C. Lo, H.S. Yu, A. Parakh, M. Patino, A. Kambadakone, E.J. Rummeny, D.V. Sahani, Material density iodine images in dual-energy CT: detection and characterization of hypervascular liver lesions compared to magnetic resonance imaging, Eur. J. Radiol. 95 (2017) 300–306, https://doi.org/10.1016/j.ejrad.2017.08.035.

[21] E.N. Milne, E.A. Zerhouni, Blood supply of pulmonary metastases, J. Thorac. Imaging 2 (1987) 15–23 (accessed May 8, 2018), http://www.ncbi.nlm.nih.gov/pubmed/2446003.

[22] E.N. Milne, A.R. Margulis, C.D. Noonan, J.T. Stoughton, Histologic type-specific vascular patterns in rat tumors, Cancer 20 (1967) 1635–1646 (accessed May 9, 2018), http://www.ncbi.nlm.nih.gov/pubmed/6058172.

[23] I.-M. Danet, R.C. Semelka, P. Leonardou, L. Braga, G. Vaidean, J.T. Woosley, M. Kanematsu, Spectrum of MRI appearances of untreated metastases of the liver, Am. J. Roentgenol. 181 (2003) 809–817, https://doi.org/10.2214/ajr.181.3.1810809.

[24] J.H. Oliver, R.L. Baron, M.P. Federle, B.C. Jones, R. Sheng, Hypervascular liver metastases: do unenhanced and hepatic arterial phase CT images affect tumor detection? Radiology. 205 (1997) 709–715, https://doi.org/10.1148/radiology.205.3.9393525.

[25] I.-M. Danet, R.C. Semelka, P. Leonardou, L. Braga, G. Vaidean, J.T. Woosley, M. Kanematsu, Spectrum of MRI appearances of untreated metastases of the liver, Am. J. Roentgenol. 181 (2003) 809–817, https://doi.org/10.2214/ajr.181.3.1810809.

[26] S.J. Swensen, R.W. Viggiano, D.E. Midthun, N.L. Müller, A. Sherrick, K. Yamashita, D.P. Naidich, E.F. Patz, T.E. Hartman, J.R. Muhm, A.L. Weaver, Lung nodule enhancement at CT: multicenter study, Radiology 214 (2000) 73–80, https://doi.org/10.1148/radiology.214.1.r00ja1473.

[27] Y.J. Jeong, K.S. Lee, S.Y. Jeong, M.J. Chung, S.S. Shim, H. Kim, O.J. Kwon, S. Kim, Solitary pulmonary nodule: characterization with combined wash-in and washout features at dynamic multi–detector Row CT, Radiology 237 (2005) 675–683, https://doi.org/10.1148/radiol.2372041549.

[28] J. Altenbernd, A. Wetter, L. Umutlu, S. Hahn, A. Ringelstein, M. Forsting, T. Lauenstein, Dual-energy computed tomography for evaluation of pulmonary nodules with emphasis on metastatic lesions, Acta Radiol. 57 (2016) 437–443, https://doi.org/10.1177/0284185115582060.

[29] J.H. Oliver, R.L. Baron, M.P. Federle, B.C. Jones, R. Sheng, Hypervascular liver metastases: do unenhanced and hepatic arterial phase CT images affect tumor detection? Radiology 205 (1997) 709–715, https://doi.org/10.1148/radiology.205.3.9393525.

[30] M.N. Levine, M.F. Drummond, R.J. Labelle, Cost-effectiveness in the diagnosis and treatment of carcinoma of unknown primary origin, CMAJ 133 (1985) 977–987 (accessed November 25, 2018), http://www.ncbi.nlm.nih.gov/pubmed/3933808.

[31] D.V. Schapira, A.R. Jarrett, The need to consider survival, outcome, and expense when evaluating and treating patients with unknown primary carcinoma, Arch. Intern. Med. 155 (1995) 2050–2054 (accessed November 25, 2018), http://www.ncbi.nlm.nih.gov/pubmed/7575063.

[32] H.K. Weir, C.J. Johnson, T.D. Thompson, The effect of multiple primary rules on population-based cancer survival, Cancer Causes Control. 24 (2013) 1231–1242, https://doi.org/10.1007/s10552-013-0203-3.

[33] J. Crow, G. Slavin, L. Kreel, Pulmonary metastasis: a pathologic and radiologic study, Cancer 47 (1981) 2595–2602 (accessed May 11, 2018), http://www.ncbi.nlm.nih.gov/pubmed/7260854.

[34] Y.J. Jeong, K.S. Lee, S.Y. Jeong, M.J. Chung, S.S. Shim, H. Kim, O.J. Kwon, S. Kim, Solitary pulmonary nodule: characterization with combined wash-in and washout features at dynamic Multi–Detector Row CT, Radiology. 237 (2005) 675–683, https://doi.org/10.1148/radiol.2372041549.

[35] W.S. Hou, H.W. Wu, Y. Yin, J.J. Cheng, Q. Zhang, J.R. Xu, Differentiation of lung cancers from inflammatory masses with dual-energy spectral CT imaging, Acad. Radiol. 22 (2015) 337–344, https://doi.org/10.1016/j.acra.2014.10.004.

[36] S. Khanduri, S. Bhagat, P. Shokeen, G. Kumar, S. Khanduri, B. Singh, Rationale of using dynamic imaging for characterization of suspicious lung masses into benign or malignant on contrast enhanced multi detector computed tomography, J. Clin. Imaging Sci. 7 (2017) 24, https://doi.org/10.4103/jcis.JCIS_18_17.

[37] H. Gong, K. Zhang, L.-M. Wu, B.F. Baigorri, Y. Yin, X. Geng, J.-R. Xu, J. Zhu, Dual energy spectral CT imaging for colorectal cancer grading: a preliminary study, PLoS One 11 (2016) e0147756, , https://doi.org/10.1371/journal.pone.0147756.

[38] L.-Y. Lin, Y. Zhang, S.-T. Suo, F. Zhang, J.-J. Cheng, H.-W. Wu, Correlation between dual-energy spectral CT imaging parameters and pathological grades of non-small cell lung cancer, Clin. Radiol. 73 (2018) 412.e1–412.e7, https://doi.org/10.1016/j.crad.2017.11.004.

[39] W. Wu, C. Parmar, P. Grossmann, J. Quackenbush, P. Lambin, J. Bussink, R. Mak, H.J.W.L. Aerts, Exploratory study to identify radiomics classifiers for lung cancer histology, Front. Oncol. 6 (2016) 71, https://doi.org/10.3389/fonc.2016.00071.

[40] J. Ma, Q. Wang, Y. Ren, H. Hu, J. Zhao, Automatic lung nodule classification with radiomics approach, in: J. Zhang, T.S. Cook (Eds.), International Society for Optics and Photonics, 2016, p. 978906, , https://doi.org/10.1117/12.2220768.

[41] T. Peikert, F. Duan, S. Rajagopalan, R.A. Karwoski, R. Clay, R.A. Robb, Z. Qin, J. Sicks, B.J. Bartholmai, F. Maldonado, Novel high-resolution computed tomography-based radiomic classifier for screen-identified pulmonary nodules in the national lung screening trial, PLoS One 13 (2018) e0196910, , https://doi.org/10.1371/journal.pone.0196910.